Investigation of oxygen dissociation and vibrational relaxation at temperatures 4000–10 800 K

L. B. Ibraguimova,[a] A. L. Sergievskaya, V. Yu. Levashov, O. P. Shatalov, Yu. V. Tunik, and I. E. Zabelinskii
Institute of Mechanics of Moscow State University, 119192 Moscow, Russia

(Received 26 March 2013; accepted 21 June 2013; published online 18 July 2013)

The oxygen absorbance was studied at wavelengths 200–270 nm in Schumann-Runge system behind the front of a strong shock wave. Using these data, the vibrational temperature T_v behind the front of shock waves was measured at temperatures 4000–10 800 K in undiluted oxygen. Determination of T_v was based on the measurements of time histories of absorbance for two wavelengths behind the shock front and on the results of detail calculations of oxygen absorption spectrum. Solving the system of standard quasi-one-dimensional gas dynamics equations and using the measured vibrational temperature, the time evolution of oxygen concentration and other gas parameters in each experiment were calculated. Based on these data, the oxygen dissociation rate constants were obtained for thermal equilibrium and thermal non-equilibrium conditions. Furthermore, the oxygen vibrational relaxation time was also determined at high temperatures. Using the experimental data, various theoretical and empirical models of high-temperature dissociation were tested, including the empirical model proposed in the present work. © *2013 AIP Publishing LLC*. [http://dx.doi.org/10.1063/1.4813070]

INTRODUCTION

The processes in high-temperature gas at thermal non-equilibrium conditions cannot be described by a single temperature. Behind the front of a strong shock wave, the vibrational temperature of molecules changes depending on the interaction of vibrational relaxation and dissociation. The quantitative experimental data on the vibrational temperature of dissociating molecules are informative characteristics for evaluation of relationship between the rates of vibrational relaxation and dissociation, and for the development of suitable theoretical models of these processes. The evident lack of such data has already resulted in a catastrophic increase in the number of various dissociation models.[1]

At the same time, no model of the thermal non-equilibrium dissociation presented in Ref. 1 has been tested because of lack of high-temperature experimental kinetic data which would allow it to make. The same situation in the available literature remains up to now. The data on the temporal evolution of the vibrational temperature of dissociating oxygen molecules and the dissociation rate constants at $T_v \neq T$ (T is the translational temperature) presented in our paper are unique. They make it possible to test both previous and new models using real experimental data.

In the present study, determination of oxygen vibrational relaxation times and dissociation rate constants, under thermal and chemical non-equilibrium conditions, is based on the data[2,3] on vibrational temperature profiles behind the shock wave front. In turn, the determination of vibrational temperature was based on simultaneous measurement of light absorption by O_2 molecules in the region of two different wavelengths in the UV spectrum (Schumann-Runge system, transition $X^3\Sigma_g^- \rightarrow B^3\Sigma_u^-$, λ = 200–270 nm), and the known oxygen absorption cross-sections $\sigma(\lambda, T, T_v)$ at high temperatures.[2]

Early experimental studies of the Schumann-Runge system, usually performed at room temperature, were reviewed in Refs. 4 and 5 (and references therein). In later studies, absorption cross-sections of oxygen were measured at higher temperatures: the measurements in Refs. 6–8 were performed up to 575 K, and in Refs. 9–15 temperatures up to 10 000 K were achieved using shock tubes.

The data on absorption cross-sections of oxygen measured in earlier high temperature experiments[9–14] were analyzed in work.[15] The analysis showed noticeable differences in absorption cross-sections measured by different authors at the same temperatures. The best agreement between the results was observed for absorption cross-sections measured under conditions of optically thin layer of gas, and the largest difference was observed for absorbance of 60%–90%, i.e., under conditions when the gas layer is not optically thin, and the Beer law is inapplicable. Thus, in our previous work[15,16] new measurements of the absorption cross-section of oxygen molecules were made under strict control of the optical thickness of the gas layer, in the spectral range 190–270 nm and in a wide temperature range.

The data on the simulation of O_2 absorption spectrum at high temperatures that were obtained in work[9] relied on approximate formulas from Ref. 5 for vacuum ultraviolet spectral range. As the method of vibrational temperature determination in the present investigation is based on the comparison between measured and calculated absorption characteristics of oxygen, it was necessary to have code that would perform reliable and detailed calculations of absorption and radiation spectra at wide ranges of wavelengths and temperatures. For this purpose the code "Spectrum"[17] was

[a]Author to whom correspondence should be addressed. Electronic mail: li@imec.msu.ru

developed. For each wavelength the absorption coefficient was simulated by the summation of absorption coefficients of rotational lines over all the feasible vibration-rotation transitions including the transitions into the continuum spectrum. In the code, both the bound-bound and bound-free transitions are taken into account, as well as the vibrational-rotational interaction for each energy state in calculations of wave functions, the non-equilibrium of gas with three molecular temperatures (electronic T_e, vibrational T_v, rotational T_r), and the instrument function for correlation between simulated and experimental spectra. Accounting for the vibrational-rotational interaction leads to a correction of the absorption cross-section in continuum from 10% to 50% at different parts of the spectrum compared to Ref. 9. With increase in temperature, the influence of vibrational-rotational interaction increases.

It is known that the dominant contribution to the absorbance of an oxygen molecule at wavelengths 140–350 nm is connected to the transitions in the Schumann-Runge system.[8,18,19] Transitions to other low-lying electronic terms ($A^3\Sigma_u^+$, $A'^3\Delta_u$, $c^1\Sigma_u^-$, $b^1\Sigma_g^+$, $a^1\Delta_g$) are forbidden. The absorption related to the transition ($1^3\Pi_u \leftarrow X^3\Sigma_g^-$) is significant for wavelengths $\lambda < 140$ nm. Wavelengths of the transition $2^3\Pi_g \leftarrow X^3\Sigma_g^-$ coincide with long-wave part of Schumann-Runge bands, however the absorption in this electronic transition is weaker by several orders of magnitude.[20] Therefore, the calculations of absorption spectra in Ref. 17 were performed only for the transitions in the Schumann-Runge system.

The calculations of absorption cross-sections were carried out for wavelengths 190–310 nm. Under conditions of thermal non-equilibrium, temperature dependences of absorption cross-section σ_λ (T_v, $T_r = T_e = T$) were obtained at temperatures from 300 to 11 000 K and it was shown that the shape of the absorption spectrum is characterized mainly by the vibrational temperature.[17]

To test the obtained spectrum model and validate the method of vibrational temperature determination, the results of simulation[17] were compared with measured absorption cross-sections.[16] The testing showed satisfactory agreement between the simulated and experimental data. This allowed the use of the calculated cross-sections at higher temperatures, for which experimental data are not available, and to measure the evolution of vibrational temperature in these conditions. In turn, this made it possible to calculate other gas parameters, to determine the dissociation rate constants, both under thermal equilibrium and thermal non-equilibrium conditions, and the vibrational relaxation time of oxygen at temperatures 6000–10 800 K. Some theoretical and empirical models of high-temperature dissociation were also tested.

EXPERIMENTAL TECHNIQUES

Our experiments were carried out in a cylindrical shock tube with inner diameter of 50 mm. A high pressure chamber was filled with a stoichiometric mixture of hydrogen and oxygen (30%) diluted by helium which was ignited by an electric pulse. A low-pressure chamber, separated by a copper was filled with undiluted oxygen of purity 99.999% to a pressure of P_1 = 1–2 Torr. The leakage of the low-pressure chamber was not higher than 4×10^{-4} Torr/min. As soon as the copper membrane separating the high and low pressure chambers of the shock tube is ruptured, the shock wave propagates along the low-pressure chamber at a velocity of 3–4.5 km/s. The velocity of the shock wave V was measured by piezoelectric transducers located in the test section of the shock tube with measurement error not greater than 1%. The distance between transducers was 100 mm, and the velocity of shock wave was not changed in this interval.

By controlling the velocity of the shock wave, the initial gas temperature T_0 immediately in the shock wave front was varied in the range 4000–10 800 K, while the pressure ranged from 0.2 to 1 atm.

To measure the absorbance of oxygen molecules, probe radiation was transmitted through the test section of the shock tube with the magnesium fluoride optical windows (with slits 0.3 mm wide), and subsequently entered a monochromator with a diffraction grating 1200 lines/mm. The monochromator was set to select a narrow range of UV: either 0.85 or 1.6 nm wide. From the output of the monochromator, the radiation entered a "blind" photomultiplier (Hamamatsu R6836) sensitive to radiation in the range 120–300 nm.

The signal from the photomultiplier was sent to a multichannel pulsed oscilloscope (Ajilent Technologies HP54624A) with a band-pass of 100 MHz. The time resolution, which is determined by the parameters of the photomultiplier-oscilloscope electric circuit, was 0.03 μs. For velocities in the range 3–4.5 km/s, the time of shock front passing by the slit located on test section window was nearly 0.1 μs. This latter value defined the time resolution of the experiment. This allowed processing the absorbance curves with time step equal to $\Delta t \approx 10^{-7}$ s with certainty that the absorption measured at a certain time has no effect on absorption from the neighboring parts of the shock wave.

A typical oscillogram of the light absorption is shown in Fig. 1. The absorbance of oxygen is measured from the relation $A = 1 - I/I_0$. Here I_0 and I are the detected intensities of probe radiation before and after the passage of the shock

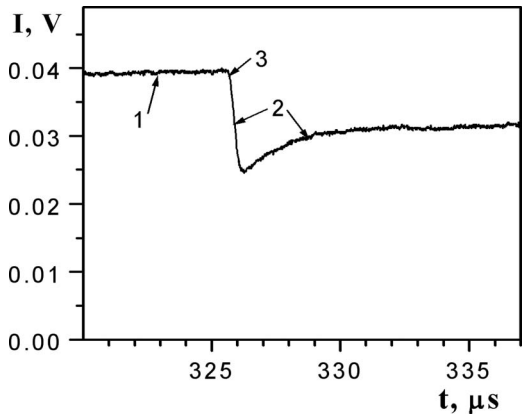

FIG. 1. Typical oscillogram of absorption at wavelength 230 nm in undiluted oxygen behind the shock front: $P_1 = 1$ Torr, $V = 4.13$ km/s, $T_0 = 9410$ K; 1 is a signal I_0 in the absence of shock wave, 2 is a signal I changed by absorption of light in heated gas, and 3 is the location of the shock wave front. Here and in other figures the abscissa is the laboratory time in microseconds.

front past the optical slits, respectively. For the optically thin gas layer, the ratio I/I_0 is described by the Beer law

$$\frac{I}{I_0} = \exp(-\sigma n l)$$

Here σ is the spectral absorption cross-section per molecule (in cm^2), l is the optical path length (in cm) in absorbing gas, i.e., the inner diameter of the shock tube, and n is the concentration of absorbing molecules (in cm^{-3}).

Absorption of oxygen in the range 190–350 nm is characterized by transitions from excited vibrational levels of the ground electronic state $X^3\Sigma_g^-$ to vibrational levels of the $B^3\Sigma_u^-$ state. As molecules are excited behind the shock wave front and vibrational levels of the $X^3\Sigma_g^-$ state are populated, the molecules begin to absorb light in the spectral range of the Schumann-Runge system. If the dissociation of molecules is significant, as soon as the absorbance reaches a certain maximum, it begins to decrease due to decrease in concentration of absorbing molecules and temperature (Fig. 1). Further, details of the experimental technique are described in Refs. 2 and 16.

EVOLUTION OF VIBRATIONAL TEMPERATURE BEHIND A SHOCK WAVE FRONT

In our study, the assumption (repeatedly verified earlier), that the low vibration levels of oxygen ground state are satisfactorily described by the harmonic oscillator model with Boltzmann distribution of populations during the vibrational relaxation and dissociation, is used. For the measurement of oxygen vibrational temperature behind the shock front, the light transmissions $(I/I_0)_1$ and $(I/I_0)_2$ were measured at two wavelengths λ_1 and λ_2 (spectral range of 200–270 nm, narrow spectral interval $\Delta\lambda \approx 1$ nm) in two separate experiments. The difference in shock velocity V, in both experiments, did not exceed 10–20 m/s. This corresponds to a difference in temperature immediately behind the shock front not higher than 120 K.

In each pair of oscillograms the wavelengths were separated by an interval from 20 to 40 nm. This made it possible to attribute the absorption at two selected wavelengths λ_1 and λ_2 to the different effective vibration levels. Under the conditions of optically thin gas layer, the vibrational temperature was determined from comparison of the measured values $\ln (I/I_0)_1 / \ln (I/I_0)_2 = (\sigma_1/\sigma_2)_{\exp}$ and the values of $(\sigma_1/\sigma_2)_{calc} = \beta(T, T_v)$ calculated in Ref. 17. It is important to note that to obtain the vibrational temperature, there is no need to know the oxygen concentration, which is an advantage of the present method. Example of vibrational temperature determination is presented in Fig. 2 for the ratio $(\sigma_1/\sigma_2)_{\exp} = 2.6$. Example of vibrational temperature determination is presented in Fig. 2 for the ratio $(\sigma_1/\sigma_2)_{\exp} = 2.6$. The processing was carried out for $T_v \le T_1 < T_0$, where the temperature T_1 was calculated on the assumption of vibration-translational equilibrium before the dissociation onset. Due to the weak dependence of σ_1/σ_2 on the temperature T, the value $T_v = f(\sigma_1/\sigma_2)$ was attributed to the translational temperature T on the range from T_0 to T_1. This yielded an error $\Delta T_v = \pm(50 \div 100)$ K at the initial time. Later this error decreased. The actual uncertainty in the determination of the vibrational temperature

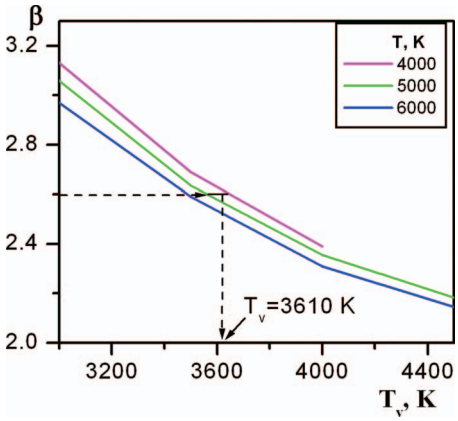

FIG. 2. Ratio of absorption cross-sections $\beta = \sigma_1/\sigma_2$ ($\lambda_1 = 240$ nm, $\lambda_2 = 260$ nm) as a function of vibrational temperature T_v at $T = 6000$, 5000, 4000, and 3000 K.

is determined by the total error in measuring velocity, initial pressure, absorption value, photomultiplier noise, the abovementioned error in the determination of T_v from plots similar to those in Fig. 2, etc. The error in the determination of T_v is mainly related to the experimental error in finding the ratio σ_1/σ_2. This error is equal to 10%–20% depending on the absorption value.[16]

Our analysis of uncertainties in the measured values made it possible to estimate the vibrational temperature measurement error. Near the front, at $T_0 < 7000$ K, the error of T_v measurement was not higher than ±10%. For high-temperature regimes ($T_0 > 7000$ K) it was equal to about ±25%, which was caused by a sharp change in absorption immediately behind the front and by the curvature of the shock. At later moments ($t_{lab} > 0.2$ μs) the error of T_v did not exceed 15%.

At the initial time, near the shock front, the error of time resolution may depend on the curvature of the front. This error was estimated in accordance with studies.[21,22] In our experiments the axial extent θ of the curved shock was 0.22–0.17 μs for shock wave velocities of 3.5–4.5 km/s, which doubled the resolution near the shock. This error decreased with time.

The examples of the vibrational temperature profiles behind the shock front are presented in Fig. 3. For each set

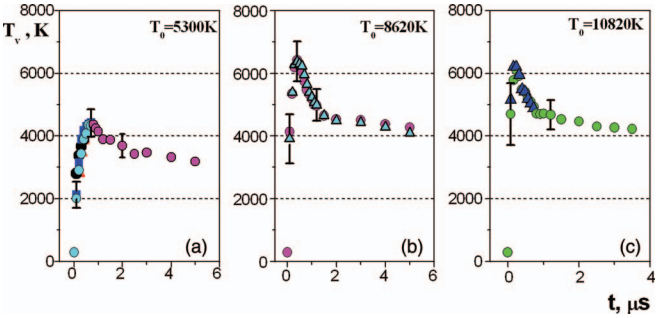

FIG. 3. Time evolution of oxygen vibrational temperature at different shock wave parameters: (a) $P_1 = 2$ Torr, $V = 3.07$ km/s, $T_0 = 5300$ K; (b) $P_1 = 1$ Torr, $V = 3.95$ km/s, $T_0 = 8620$ K; and (c) $P_1 = 0.8$ Torr, $V = 4.44$ km/s, $T_0 = 10820$ K; t is the time in laboratory coordinate system (in microseconds), Different color symbols are related to the measurements with different pairs of wavelengths: 240:260, 220:260, 230:260, and 220:250 nm.

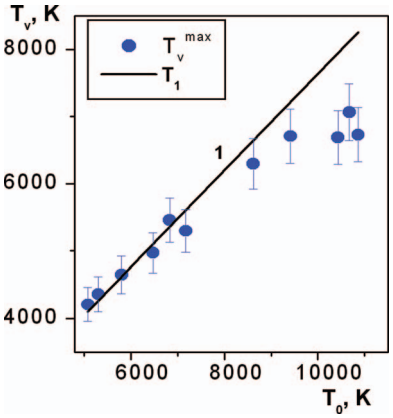

FIG. 4. Maximum vibrational temperature $T_v^{\max}$ behind the shock front vs. initial temperature T_0. Line 1 is the temperature T_1 calculated under assumption of vibration-translational equilibrium before the dissociation onset. Points are the experimental data.

of initial conditions every experimental point is obtained using absorption oscillograms corresponding to 2 or 3 different wavelengths (220–260 nm). It is seen that at initial temperatures of $T_0 < 6500$ K the measured maximum vibrational temperature $T_v^{\max}$ is attained after approximately 0.5–1.5 μs. At higher temperatures this time shortens. The chemical (thermodynamic) equilibrium is reached after a much longer period of time (some microseconds).

In the study[2] it was shown that at the temperatures $T_0 = 3500$–6500 K there is an agreement between temperature T_1 calculated under the assumption of achievement of VT – equilibrium before the onset of dissociation, and the temperature $T_v^{\max}$ measured at the absorption maximum (Fig. 4). This result confirms the well-known assumption of the separation of the vibrational relaxation and the vibrational-translational equilibrium dissociation processes of O_2 behind the shock front in the above-mentioned temperature range. At the same time it can be seen that the increase in temperature T_0 above 6000 K leads to deceleration of the growth of maximum vibrational temperature $T_v^{\max}$ (Figs. 3 and 4). Increasing T_0 up to 10 800 K leads to a difference of 1500 K between $T_v^{\max}$ and T_1 (Fig. 4). As it will be shown later, this behavior of vibrational temperature at $T_0 > 6000$–7000 K is due to the start of oxygen dissociation before the vibration-translational equilibration is attained.

DETERMINATION OF GAS PARAMETERS BEHIND THE FRONT OF A SHOCK WAVE

Behind the front of a stationary shock wave the gas flow is governed by the equations of conservation of the fluxes of mass, momentum, energy, and component composition:

$$\begin{aligned} &\rho_1 V = \rho_2 v_2, \quad P_1 + \rho_1 V^2 = P_2 + \rho_2 v_2^2, \\ &P = \rho \cdot RT \sum_i \gamma^{(i)}, \quad \frac{1}{\mu} = \sum_i \gamma^{(i)} \\ &\sum_i \gamma_1^{(i)} H_1^{(i)} + \frac{1}{2} V^2 = \sum_i \gamma_2^{(i)} H_2^{(i)} + \frac{1}{2} v_2^2 \\ &2\gamma_1^{(1)} = 0.0625 = 2\gamma_2^{(1)} + \gamma_2^{(2)}. \end{aligned} \tag{1}$$

Here, V is the shock velocity; v_2 is the gas flow velocity relative to the shock front; T, P, and ρ are the gas temperature, pressure, and density; μ is the molecular weight of the gas mixture, and H is the enthalpy of oxygen molecules and atoms. The state of the gas is denoted by the subscript 1 ahead of the shock front, and 2 behind the front. The molar-mass concentration $\gamma^{(i)}$ is represented in the form

$$\gamma^{(i)} = \frac{n^{(i)}}{\rho \cdot N_A}. \tag{2}$$

Here $n^{(i)}$ is the concentration of oxygen atoms or molecules (superscript 1 for molecules and 2 for atoms), and $N_A = 6.02 \times 10^{23}$ mole^{-1} is the Avogadro number. The enthalpy $H^{(i)}(T)$ of oxygen atoms and molecules was taken from Ref. 23. The part of the enthalpy corresponding to the vibrational energy of oxygen was represented as $\varepsilon(T) = H^{(1)}(T) - \frac{7}{2}RT$. The right side of the equation of energy conservation for the dissociating gas behind the shock front was represented in the following form:

$$\sum_i \gamma_2^{(i)} H_2^{(i)} + v_2^2/2 = \left\{H_2^{(1)}(T_2) - \varepsilon_2^{(1)}(T_2) + \varepsilon_2^{(1)}(T_v)\right\}\gamma_2^{(1)} + H_2^{(2)}\gamma_2^{(2)} + v_2^2/2.$$

Solving system (1), the gas flow parameters behind the shock front T_2, P_2, ρ_2, v_2, $\gamma_2^{(1)}$, $\gamma_2^{(2)}$ were obtained using the measured values of shock wave velocity and vibrational temperature at each selected point in time. The oxygen molecule concentration $n_2^{(1)}$ was determined from the absorption oscillograms using the Beer law and the measured vibrational temperature T_v.

The plots shown in Fig. 5 demonstrate the profiles of temperatures, density, and molar-mass concentration of O_2 for the most high-temperature regime studied in our experiments.

RATE CONSTANTS OF OXYGEN DISSOCIATION

Initially, immediately behind the front, only O_2–O_2 collisions play a role in the excitation of oxygen vibrations and dissociation. In the present work it was assumed that for degrees of oxygen dissociation less than 3%–5%, observed near the front, the role of the newborn atoms as colliding partners in oxygen dissociation was negligible. The determination of the oxygen dissociation rate constant k_d was performed under these assumptions. Recombination effects were also not taken into account. Hence, the kinetics of oxygen dissociation may be described by the simple equation,

$$\frac{d\gamma^{(1)}}{dt} = -k_d \cdot (\gamma^{(1)})^2 \cdot \rho. \tag{3}$$

The time profiles $T(t)$, $\gamma^{(1)}(t)$, and $\rho(t)$ obtained from the solution of system (1) made it possible to determine the O_2 dissociation rate constant k_d using Eq. (3) at different moments behind the shock front. The corresponding dissociation rate constants $k_d(O_2$–$O_2)$ are presented in Fig. 6 for the cases of thermal non-equilibrium ($T_v \neq T$, circles) and thermal equilibrium ($T_v = T$, triangles) conditions. The thermal non-equilibrium dissociation rate constants were obtained, when the vibrational temperature was significantly differ-

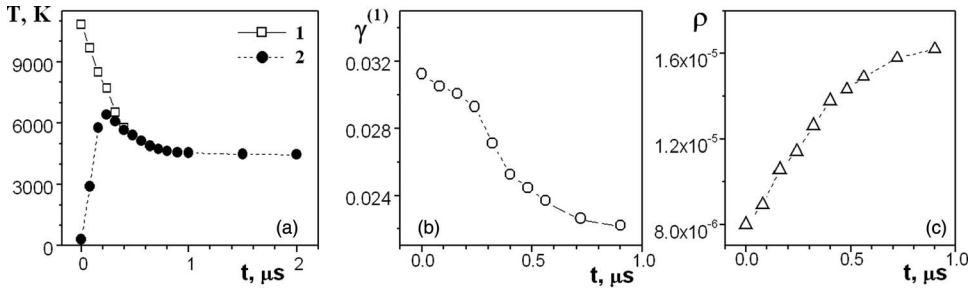

FIG. 5. Parameters of gas behind the shock front vs. time. $P_1 = 0.8$ Torr, $V = 4.44$ km/s, $T_0 = 10820$ K; (a) Profiles of translational and vibrational temperatures $T(1)$ and $T_v(2)$, K; (b) $\gamma^{(1)}$ is the O_2 molar-mass concentration, mole g^{-1}; and (c) ρ is the gas density, g cm^{-3}.

ent from the translational one. These data were obtained from the experiments with initial temperatures $T_0 = 10\,820$, 10 400, 9400, and 8620 K. For determination of thermal equilibrium values k_d^0 the experiments with $T_0 = 9400$, 8620, and 6470 K were used. They coincide with curve 4 corresponding to the recommendation[24] of thermal equilibrium dissociation rate constant.

The thermal non-equilibrium dissociation rate constants $k_d(T, T_v)$ represented in Fig. 6 by circles were obtained at different vibrational temperatures and ratios T_v/T ($0.15 < T_v/T \leq 0.7$). As can be seen, these values of $k_d(T, T_v)$ lie considerably lower than the equilibrium ones proposed in Refs. 24–26.

In Fig. 7 the rate constants $k_d(T, T_v)$ are presented as dependences of the ratio T_v/T. Numbers near the points are the translational temperatures at the same instant in which the temperature T_v was measured. As seen from the plot, the dependence of lg k_d on the ratio T_v/T is practically linear at close translational temperatures (solid lines on Fig. 7). Increase in the ratio T_v/T leads to considerable changes in the rate constant up to a factor of 3–6. This causes the scatter in the data in Fig. 6, which is much more than the uncertainty associated with experimental errors.

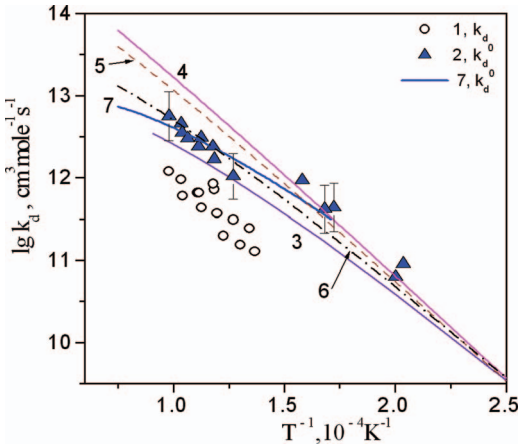

FIG. 6. Thermal equilibrium k_d^0 and thermal non-equilibrium k_d oxygen dissociation rate constant in collisions O_2–O_2. Symbols 1 and 2 correspond to the data on k_d and k_d^0, respectively. Curves 3–6 are the values k_d^0 recommended in publications: 3 – Refs. 25 and 26, 4 – Ref. 24, 5 – Ref. 27, 6 is the theoretical expression from Refs. 1 and 28, and 7 is the value k_d^0 proposed in the present study for $T > 6000$ K, (Eq. (4)).

The use of the linear dependence of lg k_d on T_v/T makes it possible to obtain the thermal equilibrium dissociation rate constant k_d^0 as the limiting values of the rate constant when the ratio T_v/T approaches unity (Fig. 7). In this way the thermal equilibrium dissociation rate constant of oxygen $k_d^0(O_2 - O_2)$ (triangles and curve 7 in Fig. 6) was obtained for temperatures 6000–11 000 K:

$$k_d^0 = 3.87 \times 10^{27}\, T^{-3.1} \cdot \exp(-59\,380/T),\ \text{cm}^3\,\text{mole}^{-1}. \tag{4}$$

In the temperature range 2000–6000 K, the expression recommended in study[24] can be used as the equilibrium rate constant k_d^0 since it satisfactorily describes experimental data including the data presented in this study:

$$k_d^0 = 2 \times 10^{15}\, T^{0.3}\,(1 - \exp(-2238/T)) \times \exp(-59380/T)\ \text{cm}^3\,\text{mole}^{-1}\,\text{s}^{-1}. \tag{5}$$

The comparison of thermal equilibrium dissociation rate constants k_d^0 recommended here (Eq. (4) and (5)) with other known data is shown in Fig. 6. One can see that at temperature $T > 6500$ K curve 7 (Eq. (5)) lies lower than the recommendations.[24,27] It is surprising that the theoretical dependence of $k_d^0(T)$ (curve 6) derived by Kuznetsov[28] (and also presented in Ref. 1) describes the experimental points rather well. The experimental data[26] (curve 3), as well as the recommendation,[25] are located slightly lower than curve 7, since the effects of thermal non-equilibrium dissociation were likely not taken into account when processing high-temperature experimental results.

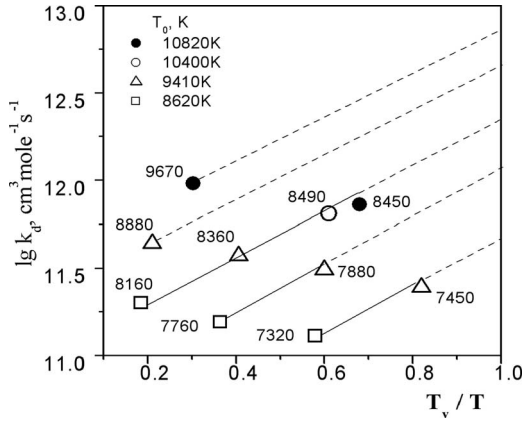

FIG. 7. Dissociation rate constant $k_d(O_2$–$O_2)$ vs. ratio T_v/T. Near each point the number is translational temperature.

Taking into account the uncertainties of the measurements and processing procedures, we can estimate the errors of the obtained values k_d and k_d^0 as $\Delta \lg k = \pm 0.3$.

MODELING OF THERMAL NON-EQUILIBRIUM DISSOCIATION

Availability of experimental data, on the evolution of the vibrational and translational temperatures, allows the testing of some theoretical and empirical models of diatomic molecules dissociation. For this purpose the well known CVDV-model of dissociation and vibrational relaxation coupling[29] was used.

$$\rho \cdot \frac{d\gamma^{(1)}}{dt} = -\sum_i k_{di} C^{(i)} C^{(1)} + \sum_i k_{ri} C^{(i)} (C^{(2)})^2, \qquad (6)$$

$$\frac{d\varepsilon}{dt} = \frac{p}{(p\tau)}(\varepsilon_0 - \varepsilon) + \frac{(E-\varepsilon)}{\gamma^{(1)}} \times \frac{d\gamma^{(1)}}{dt}. \qquad (7)$$

Here, $\gamma^{(1)}$, $\gamma^{(2)}$ are the molar-mass concentrations of O_2 and O (Eq. (2)); $C^{(i)} = \gamma^{(i)} \cdot \rho$; ε_0 and ε are the equilibrium and current vibrational energies per O_2 molecule, respectively; $(p\tau)$ is the vibrational relaxation time related to gas pressure of 1 atm; k_{di} and k_{ri} are the rate constants for the dissociation and recombination of O_2 molecules when interacting with particle i. The value k_{ri} is calculated in the form $k_{ri} = k_{di}/K_{eq}(T)$, where $K_{eq}(T)$ is the constant of thermodynamic equilibrium. The data[23] were used for its calculation. In Eq. (7) the value E is the mean vibrational energy lost in a single act of dissociation (or acquired in recombination).

In all calculations the oxygen dissociation rate constant for collisions with atoms O, $k_d(O_2\text{–}O)$ was taken to be equal to $3.5 \times k_d(O_2\text{–}O_2)$.

The mean vibrational energy E lost in dissociation is represented by different functions in different dissociation models. In the Kuznetsov model,[30] the energy E is a slightly varying value equal to $0.5\text{–}0.6 \times D_0$ (D_0 is the dissociation energy of a molecule). In the Macheret-Friedman model,[31] the energy E was not recommended at all and hence in the model in testing the value of E was assumed to be D_0. In the Hansen empirical model[32] the energy E is a constant equal to $0.33 \times D_0$.

For the description of the thermal non-equilibrium dissociation, the dissociation rate constant is represented usually in the form:

$$k_d(T, T_v) = k_d^0(T) \times Z(T.T_v)$$

where $Z(T,\ T_v)$ is the coupling factor.

The Kuznetsov model describes the dissociation of anharmonic oscillators taking into account the V–V and V–T processes. It is assumed that dissociation occurs mainly from the upper vibrational levels of the molecule and only one-quantum transitions in molecules are considered. The coupling factor is represented in the form:

$$Z^K(T, T_v) = \frac{1-\exp(-\theta/T_v)}{1-\exp(-\theta/T)} \times \exp\left[-E_v^*\left(\frac{1}{T_v} - \frac{1}{T}\right)\right].$$

It was shown that for two-atomic molecules $E_v^* \approx 0.7 \times D_0$.

In Macheret-Fridman model, two mechanisms of dissociation are considered: from upper vibrational levels of vibration-excited molecules and from low levels of non-excited molecules, when the translational energy of colliding particles is large. It only considers the dissociation of homonuclear diatomics A_2 at collisions with atoms or homonuclear diatomic B_2. The coupling factor Z in this model is described separately for collisions with molecules and atoms:

$$Z_j^{MF}(T, T_v) = \frac{1-\exp(-\theta/T_v)}{1-\exp(-\theta/T)} \times (1-L_j) \times \exp\left\{-D_0\left(\frac{1}{T_v} - \frac{1}{T}\right)\right\} + L_j \times \exp\left\{-D_0\left(\frac{1}{T_a} - \frac{1}{T}\right)\right\},$$

$$T_a^j = a_j T_v + (1-a_j)T, \quad a_j = \left(\frac{m_A}{m_A + m_B}\right)^2$$

where m_A is the mass of atom in dissociating molecule, m_B is the mass of atom-collider or the mass of atom in molecule-collider. Quantities L_j depend on the colliding partner and represent rather cumbersome expressions, given in detail in Ref. 31.

In the Hansen model the coupling factor $Z^H(T,\ T_v)$ is presented in the following form:

$$Z^H(T, T_v) = \frac{k_d}{k_d^0} = \left(\frac{T}{T_a}\right)^n \times \exp\left\{-D\left(\frac{1}{T_c} - \frac{1}{T}\right)\right\},$$

$$T_c = T^f T_v^{1-f}, \quad \text{for the } O_2 \text{ molecule } n = 1,$$

$$f = 0.85 - 0.25 \times (T_v\ /\ T).$$

In the present study an empirical model for simulation of high-temperature non-equilibrium processes behind the shock front is proposed with the following expression for the coupling factor:

$$Z = \exp\left\{-\alpha \times \left(1 - \frac{T_v}{T}\right)\right\}. \qquad (8)$$

This expression is based on the data obtained from the plots in Fig. 7.

Expressions (4) and (5) were used to compute the values of $k_d^0(T)$ for collisions $O_2\text{–}O_2$ in simulations using this model. It was assumed that the average vibrational energy E, lost by a single act of dissociation, changed during the thermal non-equilibrium dissociation. We proposed the following expression for E:

$$E = -2.5 \times \ln\left[\frac{1-\exp(-\theta/T)}{1-\exp(-\theta/T_v)} \times \frac{T_v}{T}\right] \Big/ \left\{\frac{1}{T_v} - \frac{1}{T}\right\},$$

$$T_v < T. \qquad (9)$$

This dependence is shown in Fig. 8. It can be seen, that in the most intense regimes of dissociation studied here (T_0 = 8620–10 820 K), the energy E is in the range $(0.3\text{–}0.5) \times D_0$, i.e., close to those of the Kuznetsov and Hansen models.

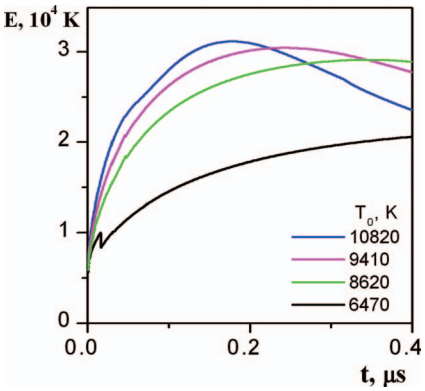

FIG. 8. Energy E (Eq. (9)) vs. laboratory time behind the front of shock wave. Numbers are the initial temperatures T_0.

If the molecule dissociates at thermal non-equilibrium conditions, it is necessary to take into account the influence of vibrational-translational non-equilibrium on the constant of thermodynamic equilibrium $K_{eq}(T)$. In the calculations this dependence was taken from study[33] for the case of Boltzmann distribution over vibrational levels:

$$K_{eq}(T, T_v) = K_{eq}(T) \times \frac{Q(T)}{Q(T_v)} \times \exp\left(-D_0\left(\frac{1}{T_v} - \frac{1}{T}\right)\right).$$

To test the dissociation models, the gas flow parameters were calculated by solving the system (1) jointly with Eqs. (6) and (7). Then, the calculated time histories (profiles) of temperatures were compared with the measured ones.

TESTING OF DISSOCIATION MODELS

The evolution of the vibrational temperature along the non-equilibrium zone is shown in Figs. 9–11. The vibrational temperature profile calculated near the shock front is the most sensitive to specified value of vibrational relaxation time, and it is weakly sensitive to the dissociation model. Hence varying $\tau_{O_2-O_2}$ allows to achieve the best fit of the calculated vibrational temperature to the one measured near he front and to obtain the values of vibrational relaxation times $\tau_{O_2-O_2}$ at high temperatures. Concentration of newborn atoms in these initial instants was negligible; however the possible influence of these atoms was taken into account. The data for $p\tau_{O_2-O}$

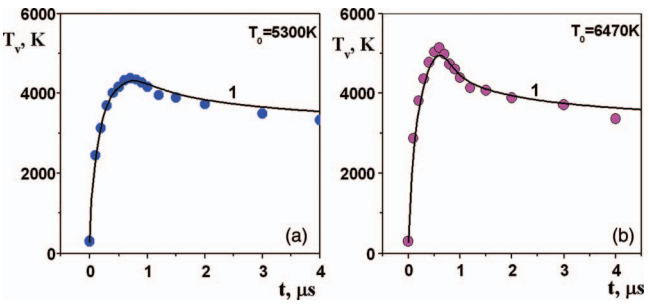

FIG. 9. Experimental data (symbols) and calculated profiles (curves) of vibrational temperature behind shock wave front at $T_0 < 7000$ K: (a) $P_1 = 2$ Torr, $V = 3.07$ km/s and (b) $P_1 = 1.5$ Torr, $V = 3.22$ km/s. Curves 1 are the results of calculations using model[30] with the value k_d^0 from Ref. 25.

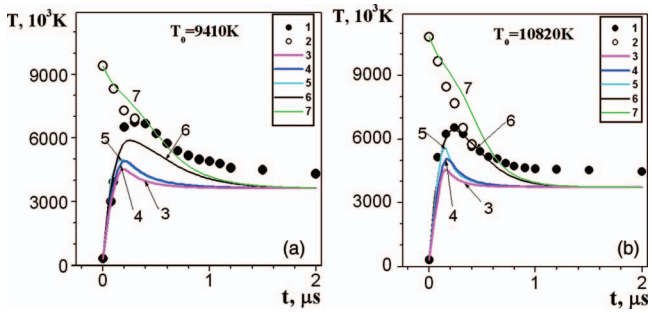

FIG. 10. Temperature profiles behind the shock wave front at $T_0 > 7000$ K. Regimes: (a) $P_1 = 1$ Torr, $T_0 = 9410$ K and (b) $P_1 = 0.8$ Torr, $T_0 = 10\,820$ K. Symbols 1 (T_v) and 2 (T) are the measured temperatures. Curves 3–6 (T_v) and 7 (T) are the results of calculations using models: 3 and 4 – Ref. 30, 5 – Ref. 32, 6 and 7 – Ref. 31. The rate constants k_d^0 were taken from Ref. 25 (4–7) and from Ref. 28 (3).

were obtained using Landau-Teller theory (see later):

$$p\tau_{O_2-O} = 1.5 \times 10^{-12} T^{0.5} \times (1 - \exp(-2238/T))^{-1} \times \exp(86.4 \cdot T^{-1/3}),\ \text{atm} \cdot \text{s}. \quad (10)$$

The data used in calculations as the quantity $p\tau_{O_2-O_2}$ are discussed later and represented by Eq. (15).

In the calculations the dissociation models described above were used. As would be expected, at temperatures less than 6500 K the models describe well the measured time history of vibrational temperature (Fig. 9). This is explained by the separation of vibrational relaxation and dissociation zones. However, with increase in temperature higher than 7000 K, none of the models[30–32] satisfactorily describes the measured temperature profiles (Fig. 10). Moreover, in experiments the thermodynamic equilibrium is established slower than predicted by these models. The moment of coincidence of the experimental vibrational and translational temperatures is observed near the maximum of the vibrational temperature for all high-temperature regimes, whereas in calculations the V–T equilibrium reached later (Fig. 10).

Figs. 11 demonstrate the results of the simulation of high-temperature oxygen dissociation behind the shock front using the empirical model (Eqs. (4), (8), and (9)). As mentioned

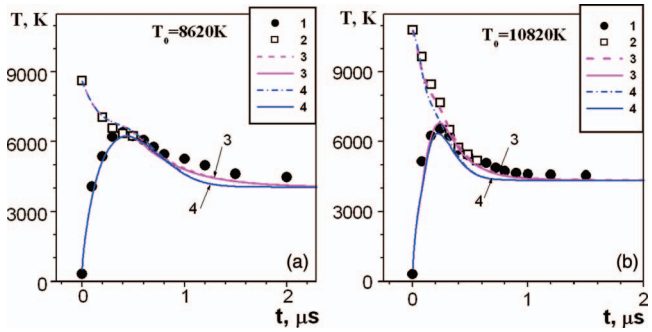

FIG. 11. Temperature profiles T_v and T behind the shock wave front at $T_0 > 7000$ K. For simulation the empirical model (Eqs. (4), (8) and (9)) was used. Regimes: (a) $P_1 = 1$ Torr, $V = 3.95$ km/s, $T_0 = 8620$ K; (b) $P_1 = 0.8$ Torr, $V = 4.44$ km/s, $T_0 = 10820$ K. Symbols 1 (T_v) and 2 (T) are the measured temperatures. Curves 3 (T, T_v) are calculated at $E = 0.45 \times D_0$, curves 4 (T, T_v) – at E described by Eq. (9).

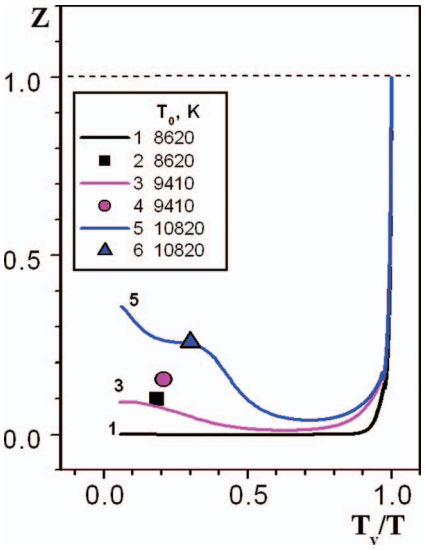

FIG. 12. Non-equilibrium factor Z vs. ratios T_v/T at different regimes. The curves 1, 3, and 5 are the simulations obtained using the empirical model. Symbols 2, 4, and 6 are the results of experimental data processing.

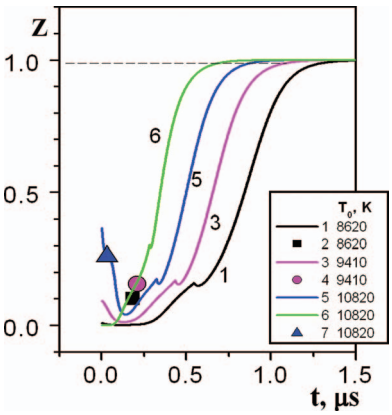

FIG. 13. Non-equilibrium factor Z vs laboratory time behind the front of the shock wave. Curves 1, 3, and 5 are simulated by empirical model, 6 is a simulation by model.[30] Symbols 2, 4, and 7 are the results of experimental data processing.

above, the parameter α in Eq. (8) depends on the temperature T and therefore using a constant value for α is a rough approximation. In light of this, the temperature dependence for α was estimated in such a way that described the temperature profiles for all high-temperature regimes accurately:

$$\alpha = 817.07 - 0.243 \cdot T + 2.42 \times 10^{-5} \cdot T^2 - 8.05 \times 10^{-10} \cdot T^3. \quad (11)$$

The use of expression (11) in Eq. (8) allowed obtaining the satisfactory agreement between simulated and measured temperature profiles in thermally non-equilibrium zone and under approaching to equilibrium. In Fig. 11 a small difference is observed between curves 3 and 4 calculated based on two different assumptions for the energy E: at constant value $E = 0.45 \times D_0$ and at time-dependent function from Eq. (9).

Figs. 12 and 13 demonstrate the evolution of the non-equilibrium factor Z given by expression (8) for three high-temperature regimes. In Fig. 12 the dependence of the factor Z on the ratio T_v/T is shown, and in Fig. 13 the factor Z is presented as a function of time. In Fig. 12 the T_v/T scale corresponds to the time scale in Fig. 13. The graphs presented in these figures show how the rate constant $k_d(T, T_v)$ changes in the thermal non-equilibrium dissociation zone depending on the model used (compare curve 6 with curves 1, 3, and 5 in Fig. 13).

Specific characteristics of the factor Z are: nonzero values at initial moments behind the front ($T_0 = 9410$ and 10 820 K), subsequent fall and then growth after a short time interval. The values Z evaluated as the ratios k_d/k_d^0 taken from experimental data at initial moments behind the shock front are shown by circles in Figs. 12 and 13. For all three regimes these values Z are also nonzero.

At high temperatures it is possible to interpret the behavior of factor Z as a change of prevalent dissociation mechanism in thermally non-equilibrium zone behind the front of the shock wave. At first, near the front, molecule dissociation occurs due to the intensive collisions characterized by the high translational temperature. At this time the factor Z is significantly different from zero, while vibrations are excited very weakly and the molecules dissociate from low vibrational levels. When translational temperature sharply falls due to dissociation, the number of such energetic collisions reduces, and at low vibrational temperature the quantity Z obtains its minimal value. Then, with the growth of vibrational temperature and population of excited vibrational levels, the prevalent dissociation mechanism becomes the dissociation from excited levels, the factor Z increases and reaches unity at thermal equilibrium. This behavior of the factor Z under increase of initial gas temperature from $T_0 = 8620$ K up to 10 820 K is shown in Figs. 12 and 13. In Fig. 13 one can see that the coupling factor calculated by the Kuznetsov model for $T_0 = 10\,820$ K (curve 6) is equal to zero initially, and shows more quick achievement of thermal equilibrium. Other models exhibit the same characteristics. In this case the simulated temperature profile does not describe the evolution of vibrational temperature observed in the experiment.

The results of the present investigation of evolution of oxygen vibrational temperature behind the front of a strong shock wave and non-equilibrium dissociation rate constants can serve as a basis for creating adequate theoretical models of the kinetics of non-equilibrium molecule dissociation.

VIBRATIONAL RELAXATION TIME

The vibrational relaxation times of most diatomic molecules collected in Millikan & White systematics[34] pertain to the low-temperature region $T \leq 2\theta$ (θ is the characteristic vibrational temperature of molecules). These data are well described by linear dependence $\lg(p\tau) = f(T^{-1/3})$ which follows from the adiabatic Landau-Teller theory.[35] The vibrational relaxation time for diatomic molecules is determined, according to Ref. 35, by the following formula:

$$p\tau = kT/[\sigma_0\sqrt{8RT/\pi\mu} \cdot pP_{10}\,(1 - \exp(-\theta/T))]. \quad (12)$$

Here σ_0 is the gas-kinetic effective cross-section of molecule collisions with particles of the medium, P_{10} is the

probability of molecule deactivation from the first vibrational level, $P_{10} \propto \exp(T^{1/3})$, and μ is the reduced molecular weight of the colliding particles.

Formula (12) represents the vibrational relaxation time of molecules at temperatures for which the main statements of the Landau-Teller theory are valid, in particular, the assumption of adiabaticity of collisions, the applicability of the harmonic oscillator model and the influence of only the repulsive part of the interaction potential on the relaxation process. It is seen from (12) that temperature dependence of the vibrational relaxation time is characterized not only by P_{10} but also by other factors which can be represented in the form:

$$u \propto \sqrt{T}/(1 - \exp(-\theta/T)). \tag{13}$$

At low temperatures ($T < 2\theta$), the quantity P_{10} depends on the temperature more strongly than does the factor u. Therefore, the dependence of $\lg(p\tau)$ on the value of $T^{-1/3}$ is almost linear. Verification of this dependence was demonstrated in work.[34]

At the same time it is clear, that neglecting other properties of molecules, such as anharmonicity, orientation of the colliding partner, the influence of attractive forces, the temperature dependence of other collision factors besides probability P_{10}, must imply a deviation of vibrational relaxation times from the Landau-Teller relationship. Even in the framework of Landau-Teller theory, increase in the temperature leads to a rapid increase of factor (13). At $T \gg 2\theta$ factor $u \propto T^{3/2}$ becomes significant and the linear dependence of $\lg(p\tau)$ on $T^{-1/3}$ inevitably breaks. Based on available experimental data expression (12) for O_2-O_2 collisions becomes

$$p\tau_{O_2-O_2} = 8.8 \times 10^{-14} \times \exp(172.7 \cdot T^{-1/3}) \times T^{0.5}/(1 - \exp(-\theta/T)),\ \text{atm s}. \tag{14}$$

In much the same way the expression (10) for O_2–O collisions was obtained. Estimates using the SSH theory[36] show little difference from the results obtained using the dependence (14).

As it was above mentioned, in the present work the data on oxygen vibrational relaxation times were obtained by fitting measured and simulated slopes of vibrational temperature profiles near the shock front. It was shown, that even small change in value τ has a considerable effect on the calculated initial slope of the vibrational temperature. This slope does not depend on the values of the dissociation rate constants nor the dissociation models used. At temperatures $T_0 < 6000$ K the initial slope of the measured profile of the vibrational temperature was satisfactorily described by means of vibrational relaxation times recommended in Ref. 34. However, for temperatures above 6000 K the rate of change of the vibrational relaxation time is slowed down compared to systematics.[34] Only once we take this phenomenon into account, can we obtain a satisfactory agreement between the calculated and the entire measured vibrational temperature profiles.

All of the data on oxygen vibrational relaxation time discussed here are presented in Fig. 14. At temperatures $T < 5000$–6000 K the experimental data are shown to be well described by Millikan-White approximation[34] (curve 1). However, at higher temperatures the quantities $\lg(p\tau)$ deviate from this dependence.[34] Accounting for pre-exponential factors, the Landau-Teller theory gives a deviation from the linear relationship (curve 2). The experimental data of the present work at $T = 6000$–$11\,000$ K are presented by magenta symbols and curve 3. The temperature dependence of this curve is following:

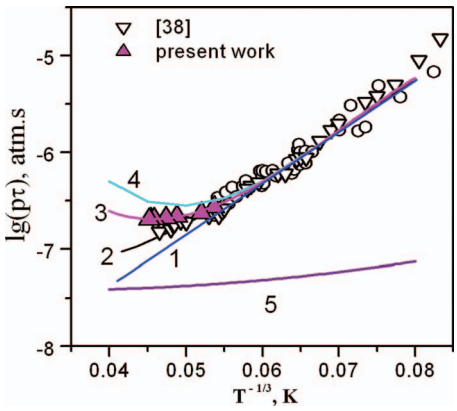

FIG. 14. Vibrational relaxation time $p\tau_{O_2-O_2}$ vs. $T^{-1/3}$. The experimental data[38] and earlier data of the authors are shown by white symbols. Magenta symbols are the results of the present work. Curves 1 and 4 are related to the data;[34,37] 2 and 5 are the values $p\tau_{O_2-O_2}$ (Eq. (14)) and $p\tau_{O_2-O}$ (Eq. (10)); 3 is the approximation of experimental data of the present study.

$$\lg p\tau = a + bx + cx^2 + dx^3, \quad x = T^{-1/3}. \tag{15}$$

Here a = 1.11, b = −407.1, c = 6600.9, and d = −31307.9.

It is interesting to note, that in the work[37] (curve 4), the oxygen vibrational relaxation time was calculated using state-to-state kinetics assuming a forced harmonic oscillator model. In this case, the discrepancy between the Landau-Teller theory and results[37] occurs at even lower temperatures. Results of work[37] appeared to be slightly greater than the experimental data.

CONCLUDING REMARKS

Measurements of the time evolution of oxygen vibrational temperature behind the front of a shock wave, presented here, showed that at $T < 6500$ K the vibrational relaxation and dissociation zones are separated. That is the vibrational-translational equilibrium is attained before the dissociation onset. At $T > 6500$ K the vibrational relaxation of molecules proceeds jointly with the dissociation already close to the shock front, i.e., the vibrational-translational equilibrium has no time to be attained before the onset of dissociation. In this case the vibrational temperature does not exceed 7000 K.

The dissociation rate constant of molecular oxygen was determined for the O_2-O_2 collisions under both thermal equilibrium and thermal non-equilibrium conditions in the temperature range from 5000 to 10 800 K. Under conditions of V–T non-equilibrium, the dissociation rate constant appreciably depends on the ratio T_v/T at the same translational temperature. The empirical model proposed here for describing the thermal non-equilibrium dissociation showed a good agreement between calculated and measured time profiles of vibrational and translational temperatures. Testing of some other

models of molecule dissociation showed that at gas temperatures above 7000 K neither of these models satisfactorily describes the measured profiles of vibrational temperature.

The vibrational relaxation times of oxygen in O_2-O_2 collisions were determined at $T = 6000–10\,800$ K. These results significantly deviates from the data, presented in popular Millikan & White systematics.[34] At the same time, at temperatures less than 6000 K recommendation[34] works well. This result is important in calculations of real gas supersonic flows where the mutual influence of vibrational relaxation and chemistry is often the determining factor in evaluation of heat transfer. The evolution of the vibrational temperature and molecule concentration obtained in the present study, allows us to describe the dissociation processes in thermally non-equilibrium conditions and to develop adequate models of these processes.

ACKNOWLEDGMENTS

The authors express their sincere gratitude to Professor A. I. Osipov, Professor A. V. Uvarov, and our colleague Dr. E. G. Kolesnichenko for useful and productive discussions. The work was supported by Grant RFBR No 10-01-00327.

[1]E. A. Kovach, S. A. Losev, and A. L. Sergievskaya, Chem. Phys. Rep. **14**, 1353 (1995).
[2]I. E. Zabelinskii, L. B. Ibraguimova, and O. P. Shatalov, Fluid Dyn. **45**, 485 (2010).
[3]I. E. Zabelinskii, L. B. Ibraguimova, O. P. Shatalov, and Yu. V. Tunik, in *Progress in Flight Physics*, Vol. 3 (Torus Press, Moscow, 2012), pp. 321–242.
[4]A. N. Zaidel and E. Ya. Shreider, *Stock Image Vacuum Ultraviolet Spectroscopy* (Ann Arbor-Humphrey Science Publishers, 1970).
[5]G. Herzberg and K.-P. Huber, *Molecular Spectra and Molecular Structure. 1. Spectra of Diatomic Molecules* (D. Van Nostrand, N.Y., 1950).
[6]S. Ogawa and M. Ogawa, Can. J. Phys. **53**, 1845 (1975)
[7]S. T. Gibson, H. P. F. Gies, A. J. Blake, D. G. McCoy, and P. J. Rogers, J. Quant. Spectrosc. Radiat. Transf. **30**, 385 (1983).
[8]J. Wang, D. G. McCoy, A. J. Blake, and R. Torop, J. Quant. Spectrosc. Radiat. Transf. **38**, 19 (1987).
[9]J. S. Evans and C. J. Schexnayder, NASA Langley Research Center, Hampton, 1961, Technical report NASA-TR-R-92.
[10]N. A. Generalov and S. A. Losev, J. Quant. Spectrosc. Radiat. Transf. **6**, 101 (1966).
[11]V. K. Dushin, I. E. Zabelinskii, and O. P. Shatalov, J. Appl. Spectrosc. **39**, 1051 (1983).
[12]V. K. Dushin, I. E. Zabelinskii, and O. P. Shatalov, Fluid Dyn. **22**, 628 (1987).
[13]S. A. Losev, O. P. Shatalov, and M. S. Yalovik, J. Appl. Spectrosc. **10**, 156 (1969).
[14]A. P. Zuev and A. Yu. Starikovskii, J. Appl. Spectrosc. **52**, 304 (1990).
[15]I. E. Zabelinskii, L. B. Ibraguimova, and O. P. Shatalov, J. Appl. Spectrosc. **73**, 10 (2006).
[16]N. G. Bykova, I. E. Zabelinskii, L. B. Ibraguimova, and O. P. Shatalov, Opt. Spectrosc. **105**, 674 (2008).
[17]N. G. Bykova and L. A. Kuznetsova, Opt. Spectrosc. **105**, 668 (2008).
[18]A. C. Allison, S. L. Guberman, and A. Dalgarno, J. Geophys. Res. **91**, 10193, doi:10.1029/JA091iA09p10193 (1986).
[19]B. R. Lewis, L. Berzins, J. H. Carven, S. T. Gibson, and D. G. McCoy, J. Quant. Spectrosc. Radiat. Transf. **34**, 405 (1985).
[20]B. R. Lewis, S. T. Gibson, and E. H. Roberts, J. Chem. Phys. **115**, 245 (2001).
[21]P. C. T. De Boer, Phys. Fluids **6**, 962 (1963).
[22]R. M. Bowman, Ph.D. dissertation, California Institute of Technology, Pasadena, 1966.
[23]*Thermodynamic Properties of Individual Substances*, edited by L. V. Gurvich and I. V. Veyts (C. B. Alcock Publisher, New York. 1989), Vol. 1, Pt. 2.
[24]L. B. Ibraguimova, G. D. Smekhov, and O. P. Shatalov, Fluid Dyn. **34**, 153 (1999).
[25]D. L. Baulch, D. D. Drysdale, J. Duxbury, and S. J. Grant, "Homogeneous gas phase reactions of the O_2-O_3 system and the CO–O_2–H_2 system, and sulfur-containing species," in *Evaluated Kinetic Data for High Temperature Reactions* (Butterworths, London, 1976), Vol. 3.
[26]O. P. Shatalov, Combust. Explos. Shock Waves **9**, 610 (1973).
[27]O. E. Krivonosova, S. A. Losev, D. P. Nalivaiko, Yu. K. Mukoseev, and O. P. Shatalov, in *Review of Plazma Chemistry*, edited by B. M. Smirnov (Consultants Bureau, New York, 1991), Vol. 1, pp. 1–29.
[28]N. M. Kuznetsov, *Kinetics of Monomolecular Reactions* (Nauka, Moscow, 1982) (in Russian).
[29]C. E. Treanor and P. V. Marrone, Phys. Fluids **5**, 1022 (1962).
[30]N. M. Kuznetsov, Theor. Exp. Chem. **7**, 17 (1973).
[31]S. A. Losev, A. L. Sergievskaya, V. D. Rusanov, A. Fridman, and S. O. Macheret, Sov. Phys. Dokl. **34**, 192 (1997).
[32]C. F. Hansen, AIAA J. **31**, 2047 (1993).
[33]A. I. Osipov and A. V. Uvarov, "Mass action law in two-temperature reacting systems," High Temp. **39**, 54 (2001).
[34]R. C. Millikan and D. R. White, J. Chem. Phys. **39**, 3209 (1963).
[35]L. Landau and E. Teller, Phys. Z. Sowjetunion **10**, 34 (1936).
[36]R. N. Schwartz and K. F. Herzfeld, J. Chem. Phys. **22**, 767 (1954).
[37]Ch. Park, AIAA Paper No. 2006-0585, 2006.
[38]S. A. Losev and N. A. Generalov, Sov. Phys. Dokl. **6**, 1081 (1962).